Available online at www.sciencedirect.com
ScienceDirect
Trans. Nonferrous Met. Soc. China 34(2024) 2645−2657
Transactions of Nonferrous Metals Society of China
www.tnmsc.cn

Graphene-loaded nickel−vanadium bimetal oxides as hydrogen pumps to boost solid-state hydrogen storage kinetic performance of magnesium hydride

Dong-qiang GAO[1], Fu-ying WU[2], Zhi ZHANG[1], Zi-chuan LU[1], Ren ZHOU[1], Hu ZHAO[3], Liu-ting ZHANG[1,3]

1. School of Energy and Power, Jiangsu University of Science and Technology, Zhenjiang 212003, China;
2. Instrumental Analysis Center, Jiangsu University of Science and Technology, Zhenjiang 212003, China;
3. School of Mechanical and Aerospace Engineering, Nanyang Technological University, Singapore 639798, Singapore

Received 6 February 2023; accepted 25 July 2023

Abstract: To modify the thermodynamics and kinetic performance of magnesium hydride (MgH_2) for solid-state hydrogen storage, $Ni_3V_2O_8$-rGO (rGO represents reduced graphene oxide) and $Ni_3V_2O_8$ nanocomposites were prepared by hydrothermal and subsequent heat treatment. The beginning hydrogen desorption temperature of 7 wt.% $Ni_3V_2O_8$-rGO modified MgH_2 was reduced to 208 °C, while the additive-free MgH_2 and 7 wt.% $Ni_3V_2O_8$ doped MgH_2 appeared to discharge hydrogen at 340 and 226 °C, respectively. A charging capacity of about 4.7 wt.% H_2 for MgH_2 + 7 wt.% $Ni_3V_2O_8$-rGO was achieved at 125 °C in 10 min, while the dehydrogenated MgH_2 took 60 min to absorb only 4.6 wt.% H_2 at 215 °C. The microstructure analysis confirmed that the in-situ generated Mg_2Ni/Mg_2NiH_4 and metallic V contributed significantly to the enhanced performance of MgH_2. In addition, the presence of rGO in the MgH_2 + 7 wt.% $Ni_3V_2O_8$-rGO composite reduced particle aggregation tendency of Mg/MgH_2, leading to improving the cyclic stability of MgH_2 during 20 cycles.

Key words: hydrogen storage properties; MgH_2; graphene-loaded Ni−V bimetal oxides; catalytic mechanism

1 Introduction

In recent decades, hydrogen energy has advanced quickly as a viable replacement for the conventional fossil fuels to address the world's energy dilemma and environmental degradation [1−3]. However, the efficient and safe storage of hydrogen remains a major obstacle to realize a hydrogen-based economy [4,5]. Because of its good capacity and security, solid-state hydrogen storage receives a huge amount of attention [6]. With the merits of high hydrogen capacity (7.6 wt.%), availability, low cost and safety, MgH_2 has been regarded as one of the best materials for solid-state hydrogen storage [7−9]. Nevertheless, sluggish kinetic characteristics and high thermo-dynamic stability of MgH_2 prevent it from being used in cars and other forms of transportation [10,11]. In order to accomplish the practical application of Mg-based composites, many investigations have been committed to resolving the inherent faults of MgH_2, including surface modification [12], nano-sizing [13,14], compositing and catalyzing [15−17].

Among the aforementioned strategies, adding catalysts to MgH_2 by means of ball-milling has been shown to be a practical and effective technique to regulate the performance of MgH_2 [18,19]. Meanwhile, the incorporation of transition metals and their complexes as catalysts is one of the most prominent studies [20]. In particular, Ni- and V-

Corresponding author: Liu-ting ZHANG, Tel: +86-15262913186, E-mail: zhanglt89@just.edu.cn;
Fu-ying WU, E-mail: wufuying@just.edu.cn; Hu ZHAO, E-mail: hu002@e.ntu.edu.sg
DOI: 10.1016/S1003-6326(24)66566-0

related catalysts can efficiently enhance the hydrogen absorption/desorption kinetics of MgH_2 [21,22]. For example, SI et al [23] found that the Mg + 5 wt.% nano-Ni composites significantly decreased the beginning desorption temperature to 180 °C and remarkably increased the absorption kinetics when compared to pure MgH_2. HUANG et al [24] prepared an efficient transition metal-based catalyst from metal organic frameworks (MOFs) and found that the Ni@C-MXene doped MgH_2 displayed high cycle stability and excellent hydrogen absorption/desorption kinetics. WANG et al [25] discovered that adding 9 wt.% V_2O_3@C could reduce the initial desorption temperature of MgH_2 from 275 to 215 °C. In addition, the MgH_2 + 9 wt.% V_2O_3@C composite could complete rehydrogenation within 3 min at 200 °C.

In addition, numerous studies demonstrated that double transition metal-based catalysts were frequently more effective than single transition metal-based catalysts for improving the hydrogen storage characteristics of MgH_2 [26−28]. For instance, MENG et al [29] revealed that the addition of $V_4Nb_{18}O_{55}$ microspheres to MgH_2 through ball milling remarkably lowered the initial dehydrogenation temperatures by about 125 °C. During rehydrogenation/dehydrogenation processes, V, Nb, NbH_2, and NbO_2 were in-situ produced, which synergistically enhanced hydrogen storage performance of MgH_2. ZHANG et al [30] observed that about 5.24 wt.% H_2 was desorbed from 5 wt.% Ni/TiO_2 doped MgH_2 within 30 min at 250 °C, while as-prepared MgH_2 could discharge 1.1 wt.% H_2 at 300 °C. Moreover, for retaining a high hydrogen storage capacity during the dehydrogenation/rehydrogenation cycles, carbon materials have been demonstrated to be effective in avoiding the agglomeration of metal nanoparticles [31,32]. LU et al [33] reported that the ability of MgH_2 + 10 wt.% TiFe to store hydrogen decreased from 6.6 wt.% to 5.8 wt.% after 10 cycles. In contrast, the hydrogen storage kinetics and content of 10 wt.% TiFe + 5 wt.% CNTs-doped MgH_2 remained steady without visible drop. JI et al [34] also revealed that the hydrogen capacity of MgH_2 + 5 wt.% FeNi/rGO was preserved even after 50 cycles without altering the cycle kinetics.

Inspired by the above encouraging results, Ni−V bimetal oxides with and without rGO were designed and synthesized using a hydrothermal technique and subsequent high-temperature calcination. Additionally, it has been established that the prepared $Ni_3V_2O_8$-rGO nanocomposite had an outstanding catalytic effect for boosting the hydrogen absorption/desorption behavior of MgH_2. Through hydrogen storage evaluation and microstructure studies, the latent catalytic mechanism of $Ni_3V_2O_8$-rGO on enhancing the hydrogen storage property of MgH_2 was discussed in detail.

2 Experimental

2.1 Synthesis of $Ni_3V_2O_8$ and $Ni_3V_2O_8$-rGO

Graphene oxide (GO) solution (5 mg/mL) was purchased from Tanfeng Tech. lnc. (Jiangsu Province, China). Orthovanadate (Na_3VO_4, AR), ammonia ($NH_3{\cdot}H_2O$, 25 wt.%) and nickel nitrate hexahydrate ($Ni(NO_3)_2{\cdot}6H_2O$, 99.9 wt.%) were acquired from Maclin and utilized without purification. By using a straightforward hydrothermal and subsequent heat treatment process, the $Ni_3V_2O_8$-rGO was synthesized. In detail, 25 mL deionized water was used to dissolve 2 mmol Na_3VO_4 at 80 °C. When the temperature of the solution was cooled to room temperature, 3 mL $NH_3{\cdot}H_2O$, 3 mmol $Ni(NO_3)_2$, and 10 mL GO (5 mg/mL) solution were gradually supplemented with continuously stirring. After that, the combined mixture was transferred to a 100 mL Tenflon-lined autoclave and maintained at 180 °C for 12 h. The acquired sample was then repeatedly rinsed with distilled water and ethanol before being cool-dried for 24 h to produce the precursor. Finally, $Ni_3V_2O_8$-rGO was obtained after the heat treatment for 3 h with floating N_2 at 450 °C. $Ni_3V_2O_8$ was prepared using an analogical procedure without GO solution.

2.2 Preparation of MgH_2-based hydrogen storage materials

MgH_2 was prepared in the laboratory [35−37]. MgH_2 was milled for 6 h in an environment of argon with x wt.% as-prepared $Ni_3V_2O_8$-rGO (x=5, 7, and 10) to get the MgH_2 + $Ni_3V_2O_8$-rGO composites. The milling speed was 400 r/min, and the ball-to-powder mass ratio was 40:1. Meanwhile, MgH_2 + 7 wt.% $Ni_3V_2O_8$ was also prepared under the similar operating conditions. All procedures were carried out in an Ar-filled glovebox to avoid contamination (high purity argon, 99.9%).

2.3 Sample characterization

The phase composition and microstructure of the specimens were investigated by X-ray diffractometer (XRD, PANalytical, the Netherlands, Cu K_a radiation), high resolution transmission electron microscope (HRTEM, JEM−2010 UHR) and transmission electron microscope (TEM, Tecnai G2 F30, operated at 300 kV) with an energy dispersive spectroscopy (EDS, M−6360LV, JEOL). Lab-made Sieverts-type device was applied to testing the experimental data of hydrogen absorption and desorption. The isothermal dehydrogenation was carried out at 215, 225, 250 and 275 °C, respectively. Meanwhile, isothermal rehydrogenation was performed at various temperatures (75, 100, 125 and 150 °C) under a starting hydrogen pressure of 3.2 MPa.

3 Results and discussion

3.1 Microstructure of as-prepared catalysts

Figure 1 presents the XRD patterns of the two obtained samples, with peaks centered at 2θ values of 18.8°, 30°, 35.9°, 36.9°, 43.3°, 57.7°, and 62.0°. The peaks matched well with the $Ni_3V_2O_8$ standard card (PDF#97-000-2646), including side peaks at around 75°. Moreover, the XRD peaks of $Ni_3V_2O_8$-rGO were wider and weaker than those of $Ni_3V_2O_8$, indicating that the crystal size of $Ni_3V_2O_8$ in $Ni_3V_2O_8$-rGO was smaller [38,39]. TEM analysis was carried out to investigate the microstructure of $Ni_3V_2O_8$-rGO nanocomposite. As shown in Fig. 2(a), it was clear that dark dots ranging from 5 to 20 nm in size were anchored to the surface of graphene layers. The SAED pattern (Fig. 2(b)) exhibited diffraction rings of (122), (042) and (442) planes, which could easily be indexed to the crystal planes of $Ni_3V_2O_8$. The interplanar spacing of 0.25 and 0.145 nm in HRTEM coincided with the (122) and (442) planes of $Ni_3V_2O_8$ (Fig. 2(c)). Besides, the EDS mapping of a selected region shown in Fig. 2(d) proved that the nanocomposites consisted of Ni, V, O, and C. Combining XRD patterns with TEM results, it is proved that $Ni_3V_2O_8$-rGO nanocomposites were successfully synthesized.

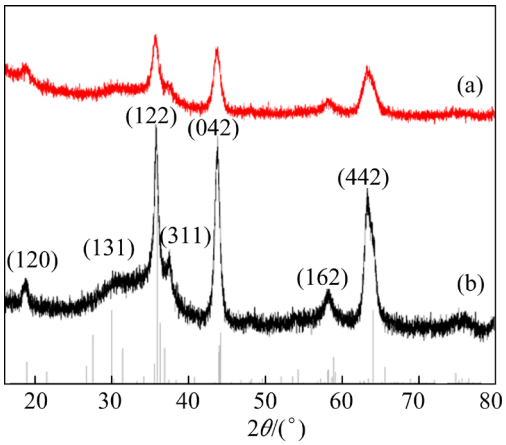

Fig. 1 XRD patterns of $Ni_3V_2O_8$-rGO (a) and $Ni_3V_2O_8$ (b) nanocomposites

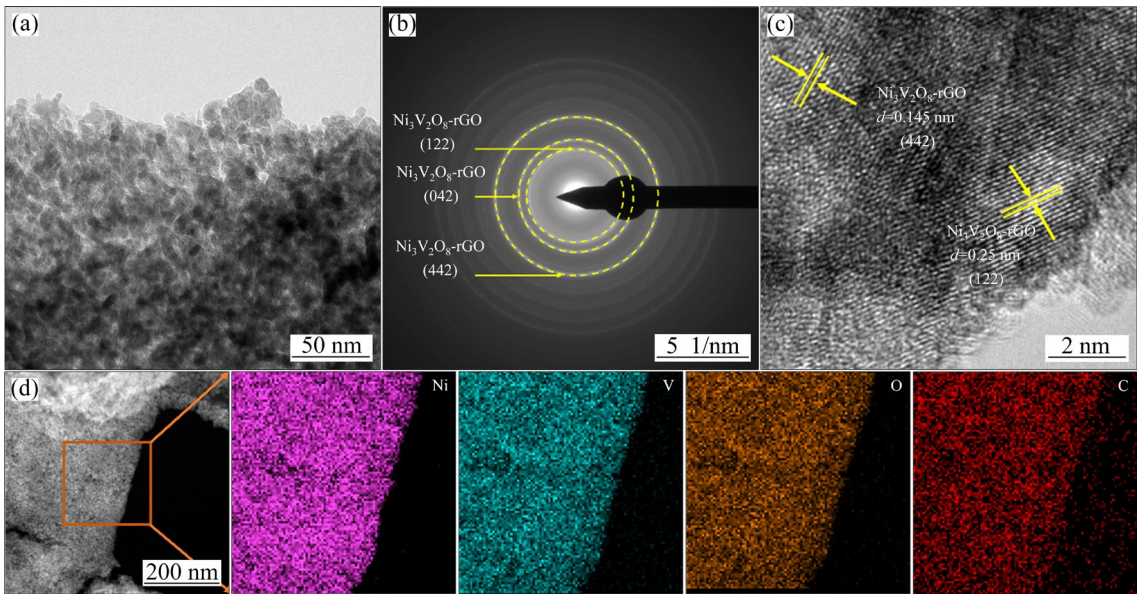

Fig. 2 TEM (a), SAED (b) and HRTEM (c) images, and STEM-HAADF image with corresponding EDS mappings (d) of as-prepared $Ni_3V_2O_8$-rGO nanocomposite

3.2 Hydrogen desorption performance of $Ni_3V_2O_8$-rGO and $Ni_3V_2O_8$ doped MgH_2

To evaluate the catalytic effects of $Ni_3V_2O_8$-rGO and $Ni_3V_2O_8$ on hydrogen desorption capabilities of MgH_2, isothermal and non-isothermal experiments were operated. The non-isothermal dehydrogenation curves of additive-free MgH_2 and MgH_2 doped with $Ni_3V_2O_8$-rGO (5 wt.%, 7 wt.%, and 10 wt.%) are shown in Fig. 3(a). It was obvious that $Ni_3V_2O_8$-rGO had a significant impact on lowering the beginning dehydrogenation temperature of MgH_2. For as-prepared MgH_2, its starting hydrogen discharge temperature was as high as 340 °C. However, the MgH_2 + 5 wt.% $Ni_3V_2O_8$-rGO, MgH_2 + 7 wt.% $Ni_3V_2O_8$-rGO, and MgH_2 + 10 wt.% $Ni_3V_2O_8$-rGO could desorb hydrogen at remarkably decreased temperatures of 217, 208, and 205 °C, respectively. Although MgH_2 + 10 wt.% $Ni_3V_2O_8$-rGO showed a 3 °C drop in the beginning dehydrogenation temperature compared to MgH_2 + 7 wt.% $Ni_3V_2O_8$-rGO, the hydrogen release rate and capacity were reduced. Considering its hydrogen desorption performance and storage capacity, MgH_2 + 7 wt.% $Ni_3V_2O_8$-rGO was chosen for the next detailed investigation. In addition, Fig. 3(b) presents the non-isothermal dehydrogenation curves of 7 wt.% $Ni_3V_2O_8$-rGO and $Ni_3V_2O_8$ doped MgH_2. The beginning dehydrogenation temperature of 7 wt.% $Ni_3V_2O_8$-rGO modified MgH_2 was further reduced to 208 °C, indicating a better catalytic effect of $Ni_3V_2O_8$-rGO over $Ni_3V_2O_8$.

To deeply investigate the influence of $Ni_3V_2O_8$-rGO and $Ni_3V_2O_8$ on the kinetic performance for MgH_2, isothermal dehydrogenation curves at various temperatures were performed (Fig. 4). It was demonstrated in Fig. 4(a) that the desorption kinetics could be greatly improved by the addition of $Ni_3V_2O_8$-rGO, which just needed less than 10 min to complete the dehydrogenation process at 250 and 275 °C, respectively. Meanwhile, around 2.2 wt.% H_2 was released within 60 min at a lower temperature of 225 °C. As shown in Fig. 4(b), the $Ni_3V_2O_8$-doped sample reluctantly discharged 0.87 wt.% H_2 and 3 wt.% H_2 at 215 and 225 °C within 1 h, respectively. Furthermore, it took about 50 min to finish the dehydrogenation process at 250 °C and 8 min at 275 °C. Figure 4(c) reveals the isothermal dehydrogenation curves of MgH_2 at 315, 335, 355, and 375 °C, respectively. At 335 °C, around 4.0 wt.% H_2 was desorbed within 25 min,

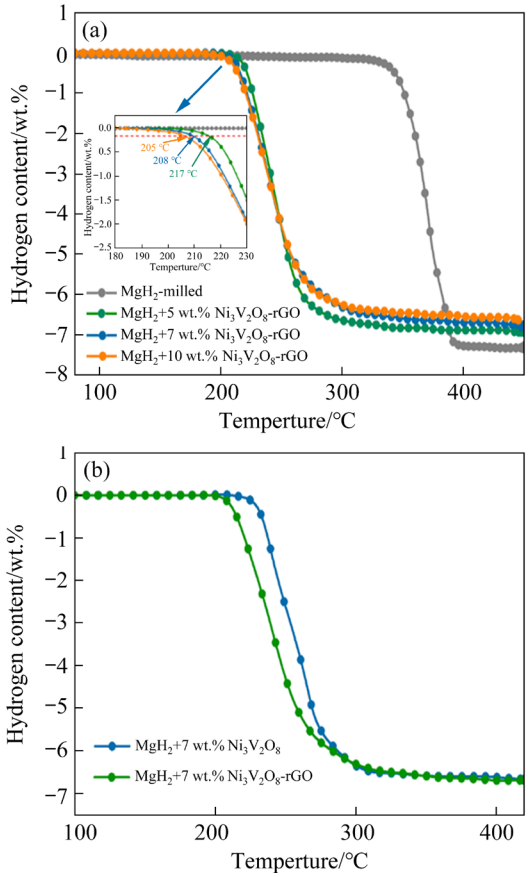

Fig. 3 Non-isothermal dehydrogenation curves of MgH_2-milled and $Ni_3V_2O_8$-rGO doped MgH_2 (a), and MgH_2 + 7 wt.% $Ni_3V_2O_8$-rGO and MgH_2 + 7 wt.% $Ni_3V_2O_8$ (b)

while it took 60 min to discharge the same amount of hydrogen at 315 °C.

To better compare the impact of $Ni_3V_2O_8$-rGO and $Ni_3V_2O_8$ on the kinetic performance of MgH_2, the isothermal dehydrogenation experiment at 250 °C was conducted (Fig. 4(d)). At 250 °C, MgH_2 + 7 wt.% $Ni_3V_2O_8$ required 38 min to discharge 6 wt.% H_2. In comparison, MgH_2 + 7 wt.% $Ni_3V_2O_8$-rGO reached the same amount of hydrogen in just 8 min. Amazingly, compared to MgH_2 + 7 wt.% $Ni_3V_2O_8$, the dehydrogenation rate for MgH_2 + 7 wt.% $Ni_3V_2O_8$-rGO was 4.15 times greater (Fig. 4(d), inset). The aforementioned experimental results demonstrated that graphene-anchored $Ni_3V_2O_8$ nanoparticles could further improve the hydrogen release capability of MgH_2. Moreover, Table 1 summarized the hydrogen release performance of various modified MgH_2 systems from published references. The MgH_2 + 7 wt.% $Ni_3V_2O_8$-rGO exhibited the best dehydrogenation property, which began to desorb hydrogen at 208 °C and released 6.3 wt.% H_2 within 10 min at 250 °C.

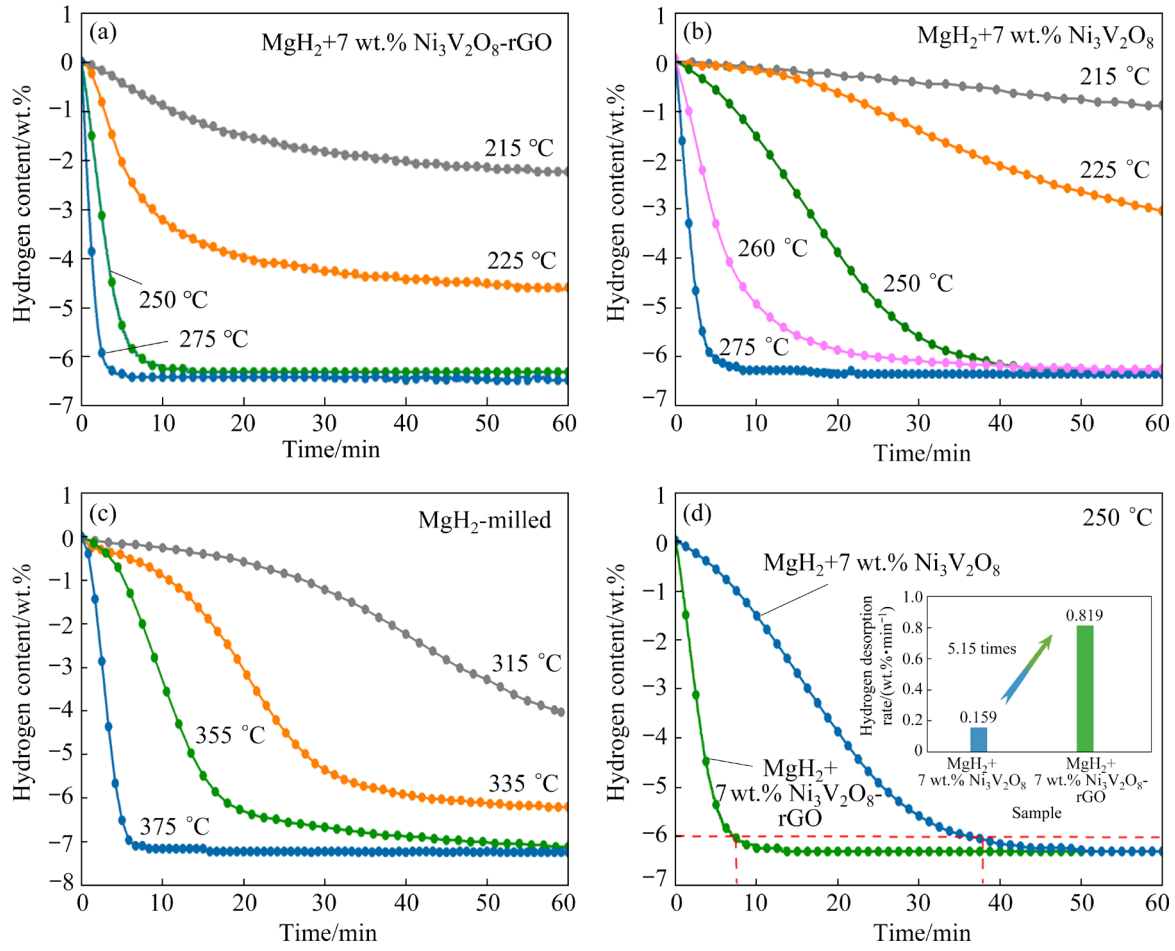

Fig. 4 Isothermal dehydrogenation curves of MgH_2 + 7 wt.% $Ni_3V_2O_8$-rGO (a), MgH_2 + 7 wt.% $Ni_3V_2O_8$ (b), MgH_2-milled (c), MgH_2 + 7 wt.% $Ni_3V_2O_8$-rGO and MgH_2 + 7 wt.% $Ni_3V_2O_8$ at 250 °C (d) (Inset in (d) shows hydrogen desorption rate for MgH_2 + 7 wt.% $Ni_3V_2O_8$-rGO and MgH_2 + 7 wt.% $Ni_3V_2O_8$)

Table 1 Dehydrogenation performance for Mg-based composites

Sample	Initial desorption temperature/°C	Isothermal dehydrogenation performance			Source
		Dehydrogenation content/wt.%	Reaction temperature/°C	Reaction time/min	
MgH_2−VB_2	250	6	275	30	[1]
MgH_2−$CoMoO_4$/rGO		5.2	250	60	[2]
MgH_2−NiO/Al_2O_3	240	4.6	275	58	[4]
MgH_2−FeOOH NDs@G	229.8	2.4	275	60	[3]
MgH_2−Ni@C-MXene	230				[17]
MgH_2−$Ni_3(VO_4)_2$	210	4.5	250	60	[27]
MgH_2−$SrFe_{12}O_{19}$	270	4.8	320	60	[28]
MgH_2−$CoTiO_3$	275				[16]
MgH_2−$Ni_3V_2O_8$-rGO	208	6.3	250	10	This work

To comprehend the improvement in kinetics, the activation energy values of MgH_2, 7 wt.% $Ni_3V_2O_8$ modified MgH_2 and MgH_2 + 7 wt.% $Ni_3V_2O_8$-rGO were calculated. In addition, the dehydrogenation activation energy (E_a) was determined using experimental data, the JMAK linear equation [40], and the Arrhenius equation [41,42]. Figures 5(a, c, e) demonstrate a strong linear relationship between

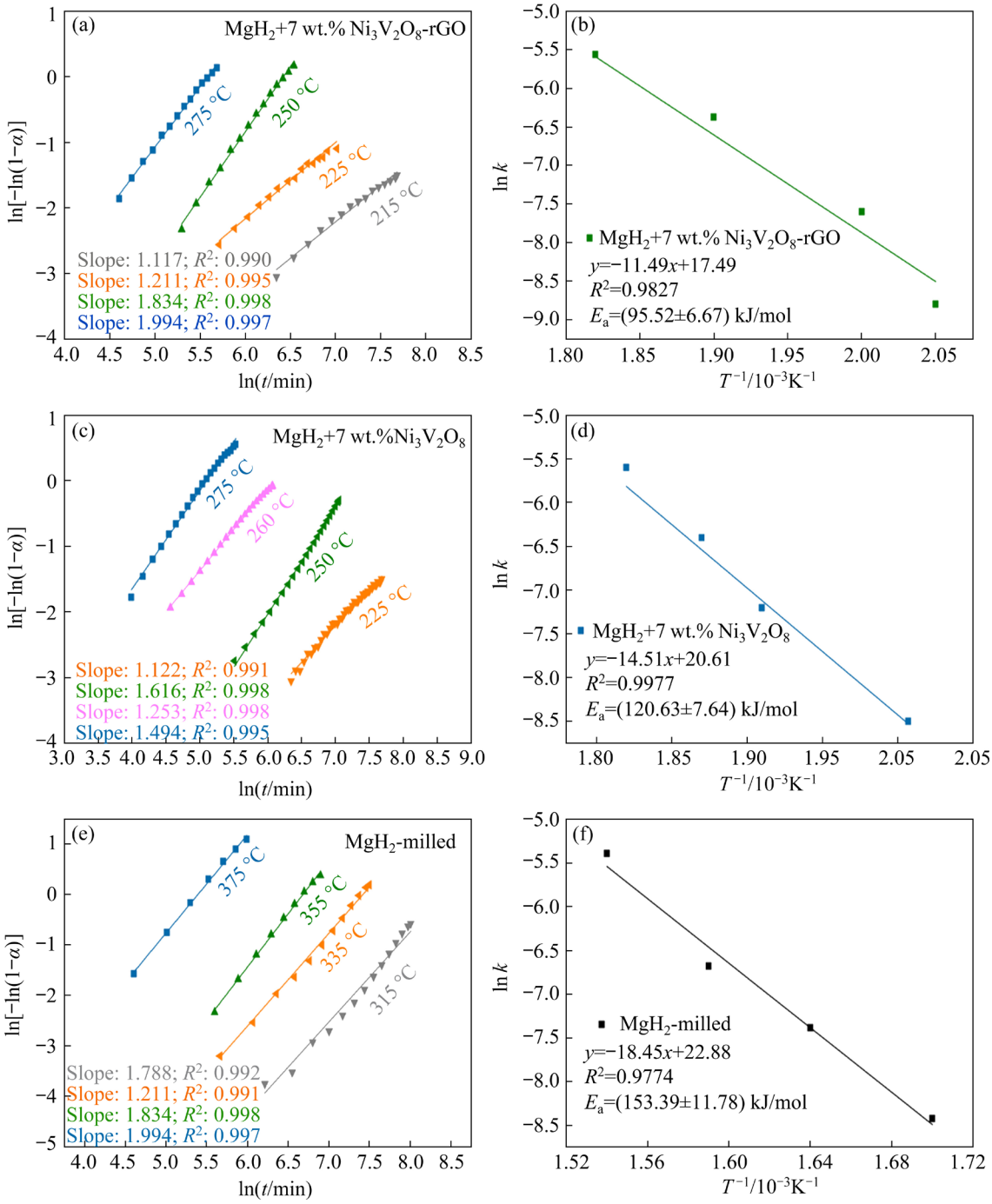

Fig. 5 JMAK plots of MgH_2 + 7 wt.% $Ni_3V_2O_8$-rGO (a), MgH_2 + 7 wt.% $Ni_3V_2O_8$ (c) and MgH_2-milled (e), and Arrhenius plots of MgH_2 + 7 wt.% $Ni_3V_2O_8$-rGO (b), MgH_2 + 7 wt.% $Ni_3V_2O_8$ (d) and MgH_2-milled (f) (α represents reaction conversion; k represents reaction rate constant)

hydrogen release capacity and time. Additionally, it was evident that dehydrogenation evolution activation energy of the prepared MgH_2 reached 153.39 kJ/mol (Fig. 5(f)). With the addition of 7 wt.% $Ni_3V_2O_8$-rGO and 7 wt.% $Ni_3V_2O_8$, the hydrogen desorption activation energies were further decreased to 95.52 and 120.63 kJ/mol (Figs. 5(b, d)).

3.3 Hydrogen absorption performance of $Ni_3V_2O_8$-rGO and $Ni_3V_2O_8$ doped MgH_2

For investigating the catalytic effect of $Ni_3V_2O_8$-rGO and $Ni_3V_2O_8$ on hydrogen absorption reaction, hydrogen absorption experiments for MgH_2 + 7 wt.% $Ni_3V_2O_8$-rGO and MgH_2 + 7 wt.% $Ni_3V_2O_8$ were conducted. Figure 6(a) compares the

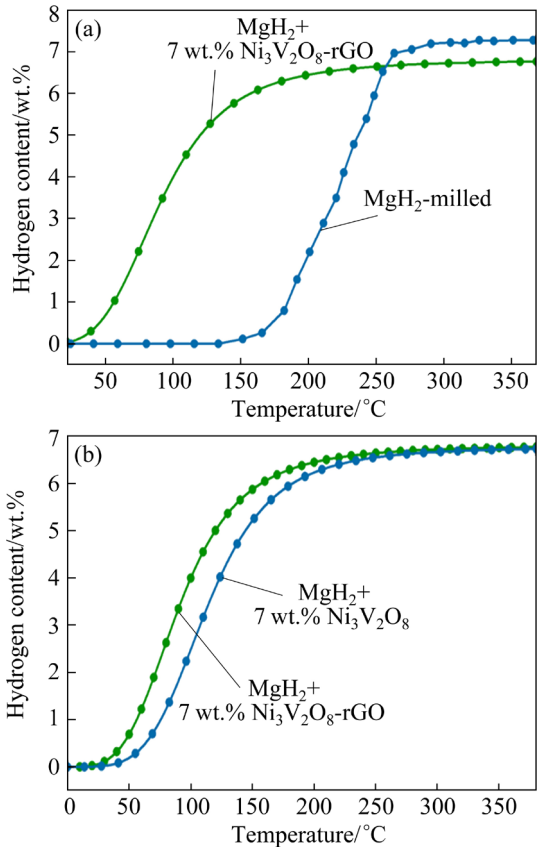

Fig. 6 Non-isothermal hydrogen absorption curves of MgH_2 + 7 wt.% $Ni_3V_2O_8$-rGO and MgH_2-milled (a), and MgH_2 + 7 wt.% $Ni_3V_2O_8$-rGO and MgH_2 + 7 wt.% $Ni_3V_2O_8$ (b)

non-isothermal hydrogen absorption results for 7 wt.% $Ni_3V_2O_8$-rGO doped MgH_2 and MgH_2-milled samples. For MgH_2 + 7 wt.% $Ni_3V_2O_8$-rGO, its initial hydrogen absorption temperature was decreased to room temperature, while MgH_2 required temperature above 140 °C before it could absorb hydrogen. When the temperature reached 150 °C during non-isothermal hydrogen absorption process, the amount of hydrogen absorbed by MgH_2 + 7 wt.% $Ni_3V_2O_8$-rGO was 5.9 wt.%. However, the as-prepared MgH_2 was reluctant to absorb hydrogen under the same condition. To investigate the influence of rGO on the catalytic effect of $Ni_3V_2O_8$, the non-isothermal rehydrogenation curves of 7 wt.% $Ni_3V_2O_8$-rGO and 7 wt.% $Ni_3V_2O_8$ modified MgH_2 were compared, as displayed in Fig. 6(b). Clearly, the MgH_2 + 7 wt.% $Ni_3V_2O_8$-rGO exhibited lower rehydrogenation temperature and faster hydrogen absorption rate. In particular, when the temperature reached 100 °C, the MgH_2 + 7 wt.% $Ni_3V_2O_8$-rGO charged 4 wt.% H_2, which was 1.5 wt.% higher than the hydrogen absorption by MgH_2 + 7 wt.% $Ni_3V_2O_8$.

To assess the hydrogen absorption kinetic performance of MgH_2 + 7 wt.% $Ni_3V_2O_8$-rGO and MgH_2 + 7 wt.% $Ni_3V_2O_8$, isothermal hydrogen absorption tests were conducted at different temperatures (Fig. 7). Furthermore, for a more perceptible comparison, the isothermal hydrogen absorption curves of MgH_2 were also compiled. As shown in Fig. 7(a), even at 75 °C, the fully dehydrogenated 7 wt.% $Ni_3V_2O_8$-rGO doped MgH_2 could charge 3.5 wt.% H_2 within 60 min. At 125 and 150 °C, the dehydrogenated MgH_2 + 7 wt.% $Ni_3V_2O_8$-rGO absorbed 4 wt.% H_2 and 5.3 wt.% H_2 within 5 min, respectively. Figure 7(b) showed that the MgH_2 + 7 wt.% $Ni_3V_2O_8$ sample could charge 2.8 wt.% H_2 within 60 min at 75 °C. When kept at 125 and 150 °C for 10 min, the composite absorbed 3.3 wt.% H_2 and 5 wt.% H_2, respectively. The pure MgH_2 required higher operating temperature to attain the equivalent rehydrogenation effect as the MgH_2 + 7 wt.% $Ni_3V_2O_8$-rGO and MgH_2 + 7 wt.% $Ni_3V_2O_8$ (Fig. 7(c)). At 215 and 235 °C, the MgH_2 demonstrated comparatively sluggish hydrogen absorption kinetics by charging 4.6 wt.% H_2 and 5.8 wt.% H_2 within 60 min. Clearly shown in Fig. 7(d), MgH_2 + 7 wt.% $Ni_3V_2O_8$-rGO charged 4.5 wt.% H_2 within 7.8 min at 125 °C, while MgH_2 + 7 wt.% $Ni_3V_2O_8$ took 34.9 min to reach the equal amount of rehydrogenation capacity under identical condition. Noteworthy, the hydrogen absorption rate of MgH_2 + 7 wt.% $Ni_3V_2O_8$-rGO was 3.48 times faster than that of 7 wt.% $Ni_3V_2O_8$ doped MgH_2 at 125 °C (Fig. 7(d), inset).

3.4 Cycling features of MgH_2 + 7 wt.% $Ni_3V_2O_8$-rGO and MgH_2 + 7 wt.% $Ni_3V_2O_8$ composites

As mentioned above, the MgH_2 + 7 wt.% $Ni_3V_2O_8$-rGO system performed superior in terms of hydrogen storage. In light of this, its cyclic stability was further assessed, which was necessary for commercial application. At 300 °C, the cycling behavior for MgH_2 + 7 wt.% $Ni_3V_2O_8$-rGO and MgH_2 + 7 wt.% $Ni_3V_2O_8$ was assessed. Figure 8(a) displays that the 7 wt.% $Ni_3V_2O_8$ doped MgH_2 was able to achieve a hydrogen content of 6.54 wt.% during the initial desorption process. However, the dehydrogenation/rehydrogenation content of 7 wt.% $Ni_3V_2O_8$ doped MgH_2 was declined to 5.90 wt.% in 20th cycle. From Fig. 8(b), MgH_2 + 7 wt.% $Ni_3V_2O_8$-rGO discharged 6.63 wt.% H_2 during the

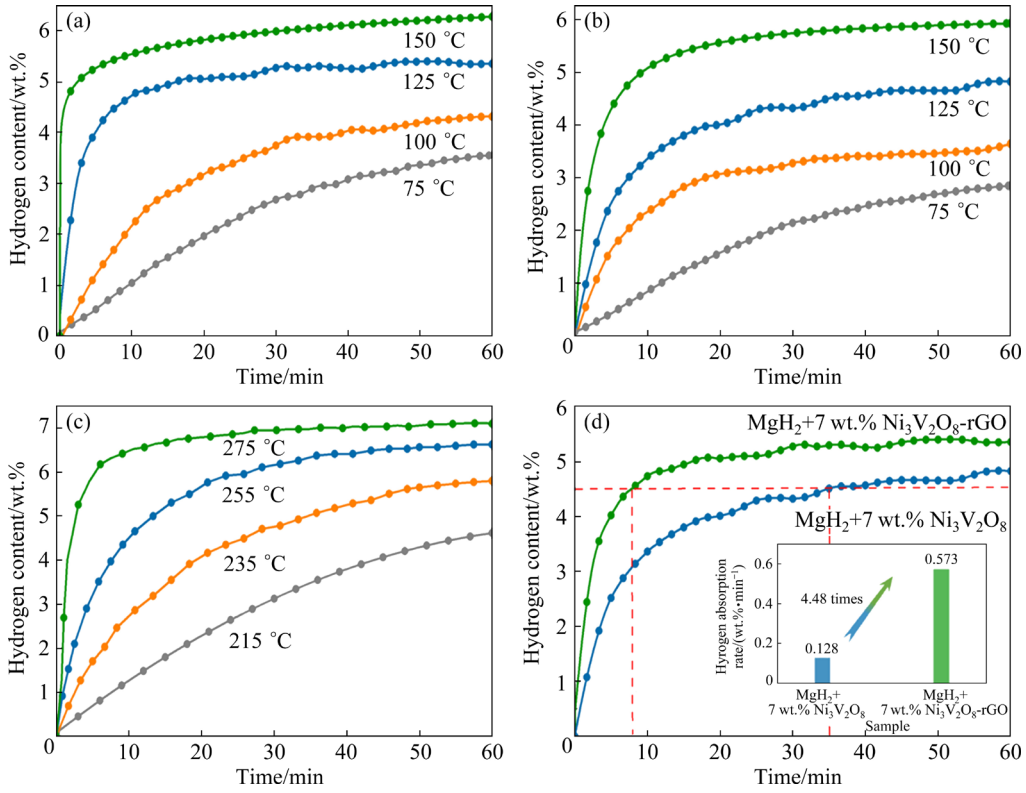

Fig. 7 Isothermal hydrogen absorption curves of MgH_2 + 7 wt.% $Ni_3V_2O_8$-rGO (a), MgH_2 + 7 wt.% $Ni_3V_2O_8$ (b), MgH_2-milled (c) at different temperatures, and MgH_2 + 7 wt.% $Ni_3V_2O_8$-rGO and MgH_2 + 7 wt.% $Ni_3V_2O_8$ at 125 °C (d) (Inset in (d) shows hydrogen absorption rate for MgH_2 + 7 wt.% $Ni_3V_2O_8$-rGO and MgH_2 + 7 wt.% $Ni_3V_2O_8$)

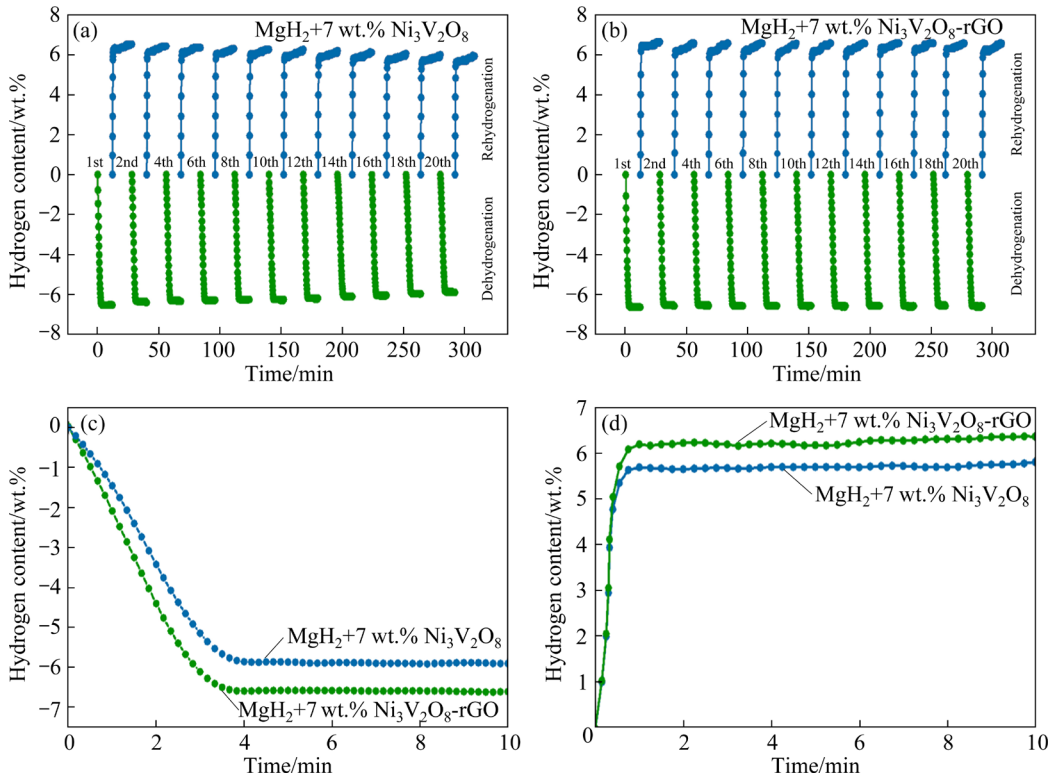

Fig. 8 Cycling curves of MgH_2 + 7 wt.% $Ni_3V_2O_8$ (a) and MgH_2 + 7 wt.% $Ni_3V_2O_8$-rGO (b) at 300 °C (3.2 MPa for absorption), and 20th dehydrogenation (c) and 20th rehydrogenation (d) curves of MgH_2 + 7 wt.% $Ni_3V_2O_8$-rGO and MgH_2 + 7 wt.% $Ni_3V_2O_8$

first cycle. After 20 cycles, the hydrogen desorption/absorption content of 7 wt.% $Ni_3V_2O_8$-rGO doped MgH_2 was maintained at 6.57 wt.%, which was 0.67 wt.% higher than that of 7 wt.% $Ni_3V_2O_8$ modified MgH_2. Additionally, Figs. 8(c) and (d) further demonstrated that MgH_2 + 7 wt.% $Ni_3V_2O_8$-rGO showed better hydrogen storage performance during 20 cycles (better dehydrogenation kinetic performance and higher hydrogen content).

3.5 Catalytic mechanism for MgH_2 + $Ni_3V_2O_8$-rGO system

As reported previously, $Ni_3V_2O_8$-rGO demonstrated exceptional catalytic action on the hydrogen storage performance of MgH_2. By using XRD and TEM to characterize the 7 wt.% $Ni_3V_2O_8$-rGO modified MgH_2, the catalytic involvement of $Ni_3V_2O_8$-rGO in the hydrogen storage reaction could be identified. Figure 9 displays the TEM, EDS, and HRTEM images of $Ni_3V_2O_8$-rGO modified MgH_2 after ball milling. As depicted in Fig. 9(a), the MgH_2 + 7 wt.% $Ni_3V_2O_8$-rGO was composed of particles that were around 500 nm in size. Furthermore, the SAED image of the sample (Fig. 9(b)) presented the $Ni_3V_2O_8$-rGO (122) and MgH_2 (111)/(220) planes, confirming that the sample was made up of MgH_2 and $Ni_3V_2O_8$-rGO. Aside from that, the HRTEM image of the selected area in Fig. 9(c) shows the interplanar spacings of 0.15 and 0.25 nm, corresponding to MgH_2 (220) and $Ni_3V_2O_8$-rGO (122) in the MgH_2 + 7 wt.% $Ni_3V_2O_8$-rGO composite, respectively. Additionally, EDS mappings of a chosen region shown in Fig. 9(d) demonstrated the existence of Mg, Ni, V, and C components in the composite, which proved the homogeneous distribution of $Ni_3V_2O_8$-rGO nanocomposite in the MgH_2 matrix. As stated in previous reports [43−45], the homogeneous distribution of C covering MgH_2 could remarkably prevent MgH_2/Mg from aggregating and growing during cycling.

For further understanding the specific mechanism of MgH_2 + 7 wt.% $Ni_3V_2O_8$-rGO composite, XRD tests were performed to identify the phase evolution. The XRD patterns for MgH_2 + 7 wt.% $Ni_3V_2O_8$-rGO in the ball-milled and rehydrogenation/dehydrogenation states are depicted in Fig. 10. In the ball-milled state, MgH_2 peaks dominated the XRD pattern. It is noteworthy that a minor MgO and $Ni_3V_2O_8$-rGO signal emerged in the magnified XRD pattern (Fig. 10(b)). MgO was largely originated from the partial reaction between MgH_2 and $Ni_3V_2O_8$-rGO during the ball milling process, which agreed well with former report [46]. In dehydrogenation, MgH_2 turned into Mg and new phases of Mg_2Ni appeared. In the rehydrogenated state, the XRD pattern was composed of peaks from MgH_2, Mg_2NiH_4, Mg and MgO. No signal of V-related compounds was identified in the rehydrogenated/dehydrogenated state, which was similar to previous references [29,46].

Combining all the above outcomes, Fig. 11 illustrates the integrated formulation on the catalytic mechanism for the $Ni_3V_2O_8$-rGO modified

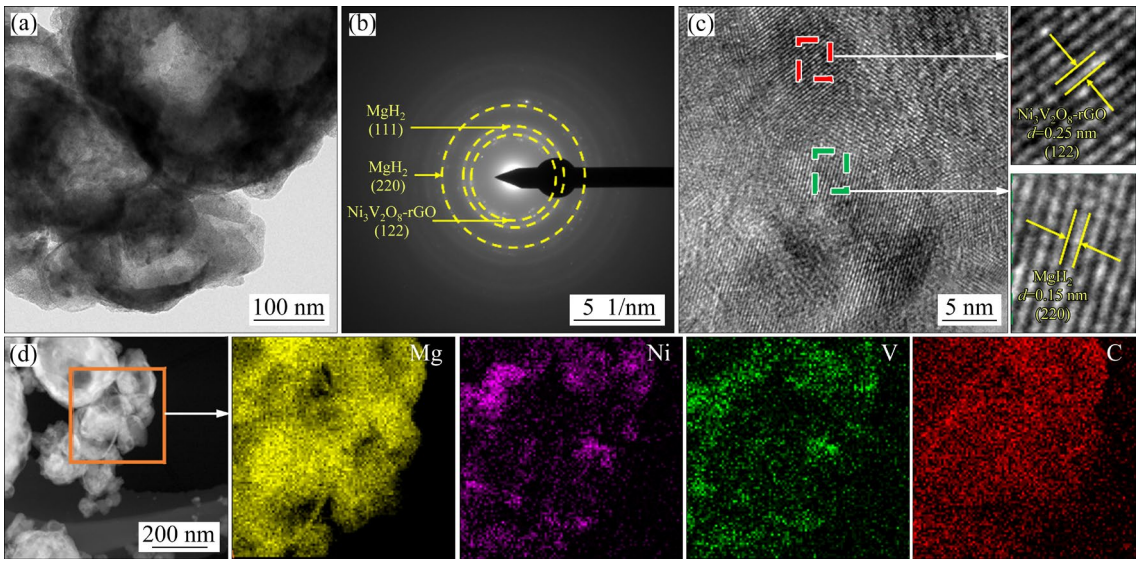

Fig. 9 TEM (a), SAED (b) and HRTEM (c) images, and STEM-HAADF image with corresponding EDS mappings (d) of MgH_2 + 7 wt.% $Ni_3V_2O_8$-rGO composite

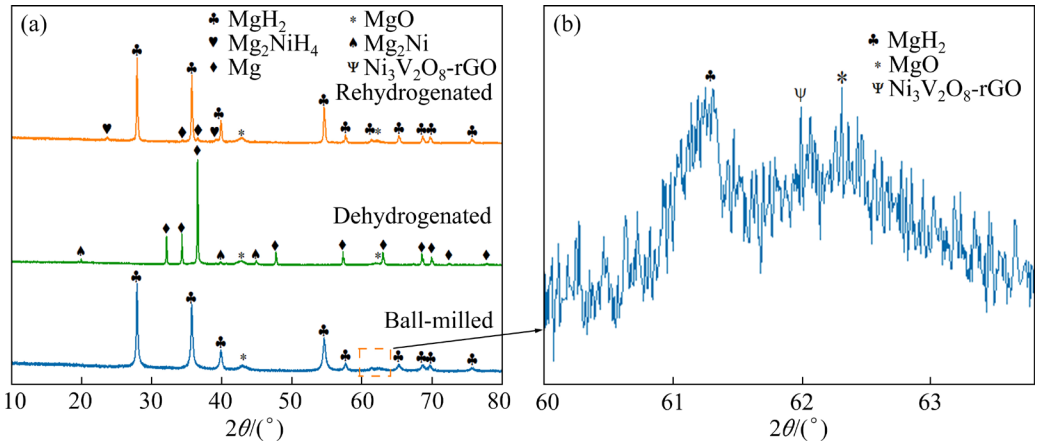

Fig. 10 XRD patterns of MgH_2 + 7 wt.% $Ni_3V_2O_8$-rGO in ball-milled, dehydrogenated and rehydrogenated states (a), and enlarged XRD patterns of ball-milled sample (b)

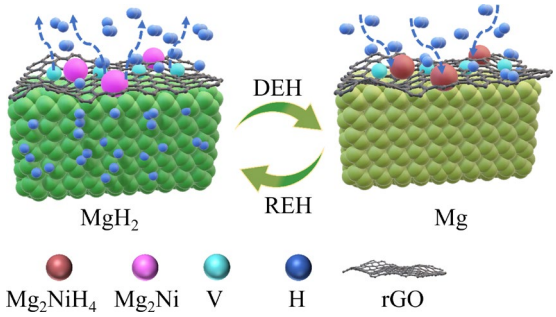

Fig. 11 Schematic diagram of catalytic mechanism for MgH_2 + 7 wt.% $Ni_3V_2O_8$-rGO composite

MgH_2 system. According to the explanation supported by the TEM images (Fig. 9), the uniformly spread $Ni_3V_2O_8$-rGO provided close contact with MgH_2, which was beneficial to exerting the catalytic action on solid-state reactions. According to earlier report [47], the density of states of MgH_2 at the Fermi level has a huge bandgap, demonstrating insulator characteristics and slow electron migration of the material. With the Mg_2Ni interface present, this significant bandgap vanished, further illuminating the transition from an insulator to a conductor [48]. Meanwhile, after introducing Mg_2Ni into the system, the Mg—H bond was elongated and it was easier to break the Mg—H bond [27]. During the process of hydrogen adsorption and desorption, the in-situ generated Mg_2Ni−Mg_2NiH_4 couples served as hydrogen pumps to accelerate the hydrogen storage kinetics of MgH_2. Similarly, V also stretched the Mg — H bonds [25] and helped to catalyze the dehydrogenation/hydrogenation reaction of MgH_2 [29,46]. At the same time, the unique rGO structure not only provided sufficient surface to anchor nanoscale $Ni_3V_2O_8$ particles, but also was beneficial to reducing the agglomeration and growth of Mg/MgH_2 particles during cycles. Thus, the superior hydrogen storage capability of the 7 wt.% $Ni_3V_2O_8$-rGO modified MgH_2 was achieved.

4 Conclusions

(1) A novel graphene-anchored Ni−V bimetal catalyst was synthesized via an easy hydrothermal and heat treatment. Furthermore, the outstanding catalytic effect of $Ni_3V_2O_8$-rGO for MgH_2 was demonstrated in detail.

(2) Specifically, the MgH_2 + 7 wt.% $Ni_3V_2O_8$-rGO began to dehydrogenate at 208 °C, 132 °C lower compared to that of as-prepared MgH_2. Meanwhile, the MgH_2 + 7 wt.% $Ni_3V_2O_8$-rGO showed superior desorption kinetics, releasing 6.3 wt.% H_2 in 10 min at 250 °C. The completely dehydrogenated 7 wt.% $Ni_3V_2O_8$-rGO modified MgH_2 could absorb hydrogen at ambient temperature and approximately 4.5 wt.% H_2 could be charged at a low temperature of 125 °C in 8 min. The MgH_2 + 7 wt.% $Ni_3V_2O_8$-rGO presented excellent cycling stability after 20 charge−discharge cycles.

(3) According to microstructure analysis, evenly scattered Mg_2Ni/Mg_2NiH_4 and metallic V enhanced the hydrogen diffusion rate at the Mg/MgH_2 interfaces, contributing to the superior solid-state hydrogen storage kinetic performance in the $Ni_3V_2O_8$-rGO modified MgH_2 system.

CRediT authorship contribution statement

Dong-qiang GAO: Investigation, Formal analysis, Writing − Review & editing; **Fu-ying WU:** Supervision, Resources; **Zhi ZHANG:** Formal analysis; **Zi-chuan LU:** Investigation; **Ren ZHOU:** Writing; **Hu ZHAO:** Project administration; **Liu-ting ZHANG:** Supervision, Resources, Writing − Review & editing.

Declaration of competing interest

The authors declare that they have no known competing financial interests or personal relationships that could have appeared to influence the work reported in this paper.

Acknowledgments

The authors appreciatively acknowledge the financial support from the National Natural Science Foundation of China (No. 51801078).

References

[1] PANG Yue-peng, WANG Yu-fang, YANG Jun-he, ZHENG Shi-you. Engineering dual-functional VB_2 nanoparticles in MgH_2 for highly efficient hydrogen storage [J]. Composites Communications, 2021, 26: 100781.

[2] ZHANG Jia-qi, HOU Quan-hui, GUO Xin-tao, YANG Xing-lin. Achieve high-efficiency hydrogen storage of MgH_2 catalyzed by nanosheets $CoMoO_4$ and rGO [J]. Journal of Alloys and Compounds, 2022, 911: 165153.

[3] SONG Meng-chen, ZHANG Liu-ting, ZHENG Jia-guang, YU Zi-dong, WANG Sheng-nan. Constructing graphene nanosheet-supported FeOOH nanodots for hydrogen storage of MgH_2 [J]. International Journal of Minerals, Metallurgy and Materials, 2022, 29: 1464−1473.

[4] LIU Zhi-bing, LIU Jiang-chuan, WU Zhao-hui, TANG Qin-ke, ZHU Yun-feng, ZHANG ji-guang, LIU ya-na, ZHANG Yao, BA Zhi-xin, HU Xiao-hui, ZHU Xin-jian, LI Li-quan. Enhanced hydrogen sorption kinetics of MgH_2 catalyzed by a novel layered Ni/Al_2O_3 hybrid [J]. Journal of Alloys and Compounds, 2022, 895: 162682.

[5] GANGU K K, MADDILA S, MUKKAMALA S B, JONNALAGADDA S B. Characteristics of MOF, MWCNT and graphene containing materials for hydrogen storage: A review [J]. Journal of Energy Chemistry, 2019, 30: 132−144.

[6] ZHU Min, LU Yan-shan, OUYANG Liu-zhang, WANG Hui. Thermodynamic tuning of Mg-based hydrogen storage alloys: A review [J]. Materials, 2013, 6: 4654−4674.

[7] LI Jing-xiao, WANG Shun, DU Yu-lei, LIAO Wen-he. Catalytic effect of Ti_2C MXene on the dehydrogenation of MgH_2 [J]. International Journal of Hydrogen Energy, 2019, 44: 6787−6794.

[8] CHEN Yan, ZHANG Hao-yu, WU Fu-ying, SUN Ze, ZHENG Jia-guang, ZHANG Liu-ting, CHEN Li-xin. Mn nanoparticles enhanced dehydrogenation and hydrogenation kinetics of MgH_2 for hydrogen storage [J]. Transactions of Nonferrous Metals Society of China, 2021, 31: 3469−3477.

[9] ZHANG Jian, HE Liu, YAO Yuan, ZHOU Xiao-jie, JIANG Li-kun, PENG Ping. Hydrogen storage properties of magnesium hydride catalyzed by Ni-based solid solutions [J]. Transactions of Nonferrous Metals Society of China, 2022, 32: 604−617.

[10] LIN Huai-jun, LU Yan-shan, ZHANG Liu-ting, LIU Hai-zhen, EDALATI K, REVESZ A. Recent advances in metastable alloys for hydrogen storage: A review [J]. Rare Metals, 2022, 41: 1797−1817.

[11] ZHANG Liu-ting, CAI Ze-liang, YAO Zhen-dong, JI Liang, SUN Ze, YAN Nian-hua, ZHANG Bei-yu, XIAO Bei-bei, DU Jun, ZHU Xin-qiao, CHEN Li-xin. A striking catalytic effect of facile synthesized $ZrMn_2$ nanoparticles on the de/rehydrogenation properties of MgH_2 [J]. Journal of Materials Chemistry A, 2019, 7: 5626−5634.

[12] PATELLI N, CALIZZI M, MIGLIORI A, MORANDI V, PASQUINI L. Hydrogen desorption below 150 °C in MgH_2−TiH_2 composite nanoparticles: Equilibrium and kinetic properties [J]. The Journal of Physical Chemistry C, 2017, 121: 11166−11177.

[13] NORBERG N S, ARTHUR T S, FREDRICK S J, PRIETO A L. Size-dependent hydrogen storage properties of Mg nanocrystals prepared from solution [J]. Journal of the American Chemical Society, 2011, 133: 10679−10681.

[14] YAO X, ZHU Z H, CHENG H M, LU G Q. Hydrogen diffusion and effect of grain size on hydrogenation kinetics in magnesium hydrides [J]. Journal of Materials Research, 2008, 23: 336−340.

[15] SHAO Yu-ting, GAO Hai-guang, TANG Qin-ke, LIU Ya-na, LIU Jiang-chuan, ZHU Yun-feng, ZHANG Ji-guang, LI Li-quan, HU Xiao-hui, BA Zhi-xin. Ultra-fine TiO_2 nanoparticles supported on three-dimensionally ordered macroporous structure for improving the hydrogen storage performance of MgH_2 [J]. Applied Surface Science, 2022, 585: 152561.

[16] ALI N A, YAHYA M S, SAZELEE N, DIN M F M, ISMAIL M. Influence of nanosized $CoTiO_3$ synthesized via a solid-state method on the hydrogen storage behavior of MgH_2 [J]. Nanomaterials, 2022, 12: 3043.

[17] ZHANG Liu-ting, YAN Nian-hua, YAO Zhen-dong, SUN Ze, LU Xiong, NYAHUMA F M, ZHU Rui-han, TU Guo-ping, CHEN Li-xin. Remarkably improved hydrogen storage properties of carbon layers covered nanocrystalline Mg with certain air stability [J]. International Journal of Hydrogen Energy, 2020, 45: 28134−28143.

[18] ZHANG Liu-ting, CHEN Li-xin, FAN Xiu-lin, XIAO Xue-zhang, ZHENG Jia-guang, HUANG Xu. Enhanced hydrogen storage properties of MgH_2 with numerous hydrogen diffusion channels provided by $Na_2Ti_3O_7$ nanotubes [J]. Journal of Materials Chemistry A, 2017, 5: 6178−6185.

[19] ZHANG Meng, XIAO Xue-zhang, WANG Xin-wei, CHEN Man, LU Yun-hao, LIU Mei-jia, CHEN Li-xin. Excellent catalysis of TiO_2 nanosheets with high-surface-energy {001} facets on the hydrogen storage properties of MgH_2 [J]. Nanoscale, 2019, 11: 7465−7473.

[20] WANG Ying, LI Li, AN Cui-hua, WANG Yi-jing, CHEN

Cheng-cheng, JIAO Li-fang, YUAN Hua-tang. Facile synthesis of TiN decorated graphene and its enhanced catalytic effects on dehydrogenation performance of magnesium hydride [J]. Nanoscale, 2014, 6: 6684−6691.

[21] LU Zhi-yu, YU Hai-jie, LU Xiong, SONG Meng-chen, WU Fu-ying, ZHENG Jia-guang, YUAN Zhi-fei, ZHANG Liu-ting. Two-dimensional vanadium nanosheets as a remarkably effective catalyst for hydrogen storage in MgH_2 [J]. Rare Metals, 2021, 40: 3195−3204.

[22] CHEN Jie, XIA Guang-lin, GUO Zai-ping, HUANG Zhen-guo, LIU Hua-kun, YU Xue-bin. Porous Ni nanofibers with enhanced catalytic effect on the hydrogen storage performance of MgH_2 [J]. Journal of Materials Chemistry A, 2015, 3: 15843−15848.

[23] SI Ting-zhi, ZHANG Xue-yang, FENG Jing-jing, DING Xiao-li, LI Yong-tao. Enhancing hydrogen sorption in MgH_2 by controlling particle size and contact of Ni catalysts [J]. Rare Metals, 2021, 40: 995−1002.

[24] HUANG Tian-ping, HUANG Xu, HU Chuan-zhu, WANG Jie, LIU Hua-bing, XU Hao, SUN Feng-zhan, MA Zhe-wen, ZOU Jian-xin, DING Wen-jiang. MOF-derived Ni nanoparticles dispersed on monolayer MXene as catalyst for improved hydrogen storage kinetics of MgH_2 [J]. Chemical Engineering Journal, 2021, 421: 127851.

[25] WANG Ze-yi, REN Zhuang-he, JIAN Ni, GAO Ming-xia, HU Jian-jiang, DU Fang, PAN Hong-ge, LIU Yong-feng. Vanadium oxide nanoparticles supported on cubic carbon nanoboxes as highly active catalyst precursors for hydrogen storage in MgH_2 [J]. Journal of Materials Chemistry A, 2018, 6: 16177−16185.

[26] XU Guang, SHEN Na, CHEN Ling-juan, CHEN Yang, ZHANG Wei. Effect of $BiVO_4$ additive on the hydrogen storage properties of MgH_2 [J]. Materials Research Bulletin, 2017, 89: 197−203.

[27] ZANG Jia-he, WANG Shao-fei, HU Rong-run, MAN Han, ZHANG Ji-chao, WANG Fei, SUN Da-lin, SONG Yun, FANG Fang. Ni, beyond thermodynamic tuning, maintains the catalytic activity of V species in $Ni_3(VO_4)_2$ doped MgH_2 [J]. Journal of Materials Chemistry A, 2021, 9: 8341−8349.

[28] MUSTAFA N S, SULAIMAN N N, ISMAIL M. Effect of $SrFe_{12}O_{19}$ nanopowder on the hydrogen sorption properties of MgH_2 [J]. RSC Advances, 2016, 6: 110004−110010.

[29] MENG Yang, JU Shun-long, CHEN Wei, CHEN Xiao-wei, XIA Guang-lin, SUN Da-lin, YU Xue-bin. Design of bifunctional Nb/V interfaces for improving reversible hydrogen storage performance of MgH_2 [J]. Small Structures, 2022, 3: 2200119.

[30] ZHANG Ji-guang, SHI Rui, ZHU Yun-feng, LIU Ya-na, ZHANG Yao, LI Shan-shan, LI Li-quan. Remarkable synergistic catalysis of Ni-doped ultrafine TiO_2 on hydrogen sorption kinetics of MgH_2 [J]. ACS Applied Materials & Interfaces, 2018, 10: 24975−24980.

[31] ZHOU Dong-mei, CUI Kai-xuan, ZHOU Zhang-wei, LIU Chun-rong, ZHAO Wang, LI Ping, QU Xuan-hui. Enhanced hydrogen-storage properties of MgH_2 by Fe−Ni catalyst modified three-dimensional graphene [J]. International Journal of Hydrogen Energy, 2021, 46: 34369−34380.

[32] DING Zhen-min, FU Yao-kun, ZHANG Lu, RODRIGUEZ-PEREZ I A, ZHANG Hong-ming, WANG Wen-feng, LI Yuan, HAN Shu-min. Improve hydrogen sorption kinetics of MgH_2 by doping carbon-encapsulated iron-nickel nanoparticles [J]. Journal of Alloys and Compounds, 2020, 843: 156035.

[33] LU Xiong, ZHANG Liu-ting, YU Hai-jie, LU Zhi-yu, HE Jia-huan, ZHENG Jia-guang, WU Fu-ying, CHEN Li-xin. Achieving superior hydrogen storage properties of MgH_2 by the effect of TiFe and carbon nanotubes [J]. Chemical Engineering Journal, 2021, 422: 130101.

[34] JI Liang, ZHANG Liu-ting, YANG Xing-lin, ZHU Xin-qiao, CHEN Li-xin. The remarkably improved hydrogen storage performance of MgH_2 by the synergetic effect of an FeNi/rGO nanocomposite [J]. Dalton Transactions, 2020, 49: 4146−4154.

[35] TIAN Gui-bin, WU Fu-ying, ZHANG Hao-yu, WEI Juan, ZHAO Hu, ZHANG Liu-ting. Boosting the hydrogen storage performance of MgH_2 by Vanadium based complex oxides [J]. Journal of Physics and Chemistry of Solids, 2023, 174: 111187.

[36] GUEMOU S, GAO Dong-qiang, WU Fu-ying, ZHENG Jia-guang, WEI Tao, YAO Zhen-dong, SHANG Dan-hong, ZHANG Liu-ting. Enhanced hydrogen storage kinetics of MgH_2 by the synergistic effect of Mn_3O_4/ZrO_2 nanoparticles [J]. Dalton Transactions, 2023, 52: 609−620.

[37] SONG Meng-chen, ZHANG Liu-ting, YAO Zhen-dong, ZHENG Jia-guang, SHANG Dan-hong, CHEN Li-xin, LI Hong. Unraveling the degradation mechanism for the hydrogen storage property of Fe nanocatalyst-modified MgH_2 [J]. Inorganic Chemistry Frontiers, 2022, 9: 3874−3884.

[38] YANG Ming-yang, FU Xue-lian, ZHANG Jian-qiao, WANG Zhen-yu, WANG Bing-xue, HE Li-qing, WU Zhi-liang, CHENG Hua, PAN Hui, LU Zhou-guang. Hierarchical ultrafine $Ni_3V_2O_8$ nanoparticles anchored on rGO as high-performance anode materials for lithium-ion batteries [J]. Energy Technology, 2019, 7: 1800784.

[39] SIBURIAN R, ALI A M M, SEBAYANG K, SUPENO M, TARIGAN K, SIMANJUNTAK C, ARITONANG S P, HUTAGALUNG F. The loading effect of Pt clusters on Pt/graphene nano sheets catalysts [J]. Scientific Reports, 2021, 11: 2532.

[40] ZHANG Jian, YAN Shuai, XIA Guang-lin, ZHOU Xiao-jie, LU Xian-zheng, YU Lin-ping, YU Xue-bin, PENG Ping. Stabilization of low-valence transition metal towards advanced catalytic effects on the hydrogen storage performance of magnesium hydride [J]. Journal of Magnesium and Alloys, 2021, 9: 647−657.

[41] HU Song, ZHANG Huan-huan, YUAN Zhen-luo, WANG Yu-hang, FAN Guang-xin, FAN Yan-ping, LIU Bao-zhong. Ultrathin $K_2Ti_8O_{17}$ nanobelts for improving the hydrogen storage kinetics of MgH_2 [J]. Journal of Alloys and Compounds, 2021, 881: 160571.

[42] LI Qian, LIN Xi, LUO Qun, CHEN Yu-an, WANG Jing-feng, JIANG Bin, PAN Fu-sheng. Kinetics of the hydrogen absorption and desorption processes of hydrogen storage alloys: A review [J]. International Journal of Minerals, Metallurgy and Materials, 2022, 29: 32−48.

[43] ZENG Liang, LAN Zhi-qiang, LI Bao-bao, LIANG Hui-ren, WEN Xiao-bin, HUANG Xian-tun, TAN Jun, LIU Hai-zhen,

ZHOU Wen-zheng, GUO Jin. Facile synthesis of a Ni_3S_2@C composite using cation exchange resin as an efficient catalyst to improve the kinetic properties of MgH_2 [J]. Journal of Magnesium and Alloys, 2022, 10: 3628−3640.

[44] HOU Quan-hui, ZHANG Jia-qi, GUO Xin-tao, XU Guan-zhong, YANG Xing-lin. Synthesis of low-cost biomass charcoal-based Ni nanocatalyst and evaluation of their kinetic enhancement of MgH_2 [J]. International Journal of Hydrogen Energy, 2022, 47: 15209−15223.

[45] ZHANG Liu-ting, SUN Ze, CAI Ze-liang, YAN Nian-hua, LU Xiong, ZHU Xin-qiao, CHEN Li-xin. Enhanced hydrogen storage properties of MgH_2 by the synergetic catalysis of $Zr_{0.4}Ti_{0.6}Co$ nanosheets and carbon nanotubes [J]. Applied Surface Science, 2020, 504: 144465.

[46] GAO Dong-qiang, ZHANG Liu-ting, SONG Meng-chen, WU Fu-ying, WANG Jiao, ZHAO Hu, LI Hong. Interfacial engineering of nickel/vanadium based two-dimensional layered double hydroxide for solid-state hydrogen storage in MgH_2 [J]. International Journal of Hydrogen Energy, 2023, 48: 9390−9400.

[47] AO Bing-yun, ZHANG Zheng-jun, HE Yu-ping, ZHAO Yi-ping. Semiconducting ground-state of three polymorphs of Mg_2NiH_4 from first-principles calculations [J]. International Journal of Hydrogen Energy, 2013, 38: 16471−16476.

[48] LI G X, LAN Z Q, TSENG Y S, ZHOU We Z, GUO J, CHAN S L I. Penetration and diffusion of hydrogen in Mg_2Ni: A first-principles investigation [J]. International Journal of Hydrogen Energy, 2017, 42: 3097−3105.

以石墨烯负载镍钒双金属氧化物作为氢泵提高氢化镁的固态储氢动力学性能

高东强[1]，吴富英[2]，张 智[1]，路紫川[1]，周 任[1]，赵 虎[3]，张刘挺[1,3]

1. 江苏科技大学 能源与动力学院，镇江 212003；

2. 江苏科技大学 分析测试中心，镇江 212003；

3. School of Mechanical and Aerospace Engineering, Nanyang Technological University, Singapore 639798, Singapore

摘 要：为了改善氢化镁(MgH_2)的固态储氢热力学和动力学性能，采用水热法和后续热处理法制备 $Ni_3V_2O_8$-rGO (rGO 为还原氧化石墨烯)和 $Ni_3V_2O_8$ 纳米复合材料。掺杂 7%(质量分数) $Ni_3V_2O_8$-rGO 的 MgH_2 的初始放氢温度降低到 208 ℃，而纯 MgH_2 和掺杂 7% (质量分数) $Ni_3V_2O_8$ 的 MgH_2 的初始放氢温度分别为 340 和 226 ℃。在 125 ℃条件下，MgH_2 + 7% $Ni_3V_2O_8$-rGO (质量分数) 在 10 min 内吸收了约 4.7% (质量分数) 的 H_2，而放氢完成后的 MgH_2 在 215 ℃条件下需要 60 min 才能吸收 4.6% (质量分数) 的 H_2。显微组织表征分析证实原位生成的 Mg_2Ni/Mg_2NiH_4 和金属态 V 显著提高了 MgH_2 的性能。此外，MgH_2 + 7% $Ni_3V_2O_8$-rGO (质量分数) 复合材料中的 rGO 减轻了 Mg/MgH_2 颗粒团聚现象，使 MgH_2 在 20 次循环中具有更好的循环稳定性。

关键词：储氢性能; MgH_2; 石墨烯负载 Ni−V 双金属氧化物; 催化机理

(Edited by Wei-ping CHEN)